


Synchronous Transition in Complex Object Control

Brent Wallace,¹ Ling-Wei Kong,¹ Armando Rodriguez,¹ and Ying-Cheng Lai^{1,2,*}

¹*School of Electrical, Computer and Energy Engineering, Arizona State University, Tempe, Arizona 85287, USA*

²*Department of Physics, Arizona State University, Tempe, Arizona 85287, USA*

 (Received 25 May 2021; revised 5 August 2021; accepted 16 August 2021; published 7 September 2021)

A complex object is a system with internal degrees of freedom, such as a cup of hot coffee hand-held by a human in walking. In spite of the natural ability of humans to handle complex objects, an understanding of how this is accomplished is lacking, yet the issue is fundamental to applied fields such as soft robotics. Recent virtual experiments on how humans handle a moving bowl with a mechanical ball inside have revealed that humans typically use two strategies to handle a complex object: a low-frequency strategy in which the motions of the bowl and ball synchronized in phase and a high-frequency strategy where antiphase synchronization occurs. Utilizing a nonlinear dynamical model of a pendulum attached to a moving cart, subject to external periodic forcing, we study the transition between in-phase and antiphase synchronization. We find that, in the weakly forcing regime, as the external driving frequency is varied, the transition is abrupt and occurs at the frequency of resonance, which can be fully understood using linear systems control theory. Beyond this regime, a transition region emerges in between in-phase and antiphase synchronization, where the motions of the cart and the pendulum are not synchronized. We also find that there is bistability in and near the transition region on the low-frequency side. Overall, our results indicate that humans are able to switch abruptly and efficiently from one synchronous attractor to another, a mechanism that can be exploited for designing smart robots to adaptively handle complex objects in a changing environment.

DOI: [10.1103/PhysRevApplied.16.034012](https://doi.org/10.1103/PhysRevApplied.16.034012)

I. INTRODUCTION

Complex objects are those with internal degrees of freedom that are not directly controlled externally. When a complex object is utilized or manipulated by a user, its internal “gears” will interact with the user in a complicated manner. The use of complex objects, e.g., various tools, has played a fundamental role in human evolution, and humans are masterful at handling and exploiting complex objects. A classic example is the ability of humans to walk at a reasonable speed while carrying a cup of hot coffee without spilling [1–3]. The hot coffee, being a thermally agitated fluid confined in the cup, has internal degrees of freedom that interact with the cup that, in turn, interacts with the human carrier. The detailed physics of the chain of interactions can be quite complex. Another example is human stick balancing, where most human individuals have no difficulty in balancing a pole at the fingertip through controlled small movements, a topic in nonlinear and stochastic dynamics pioneered by Milton and collaborators [4–8]. While humans possess a natural and “gifted” ability to interact with complex objects, our understanding of the interactions, especially at a quantitative level, is

next to zero, let alone analyzing the influences of external perturbations such as environmental noise. In spite of our present lack of understanding, a feature that is certain about the interactions is that they are nonlinear. We thus anticipate nonlinear dynamics to play an important role in unlocking and deciphering the dynamics of human interactions with complex objects, a fundamental understanding of which is essential to frontier fields such as soft robotics, rehabilitation, and brain-machine interface.

Recently, a ground-breaking virtual experimental study was conducted to examine how humans manipulate a complex object [2,3], with a focus on the classic coffee-cup holding paradigm. One goal of the study was to uncover the strategies that humans choose to handle such a complex object. For this purpose, a cart-pendulum model was articulated to mimic the dynamical interaction between the cup and the hot coffee inside. Experimentally, the model was implemented in a virtual environment where a cup of hot coffee is simulated by a virtual cup containing a rolling ball, as shown schematically in Fig. 1(a). The participants were asked to manipulate the cup in a rhythmical manner to ensure that the ball stays in the cup. The rhythmic motion is equivalent to some kind of periodic driving, and humans are able to vary the driving force and frequency continuously. In a description

*Ying-Cheng.Lai@asu.edu

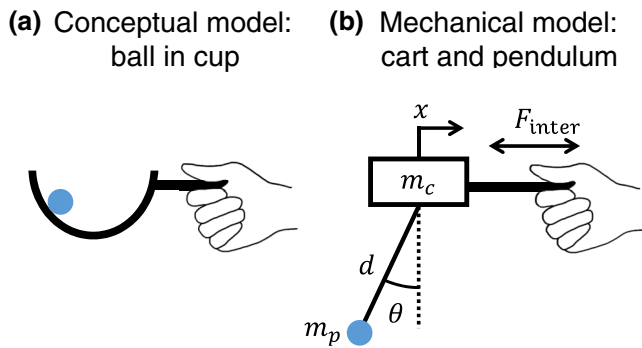


FIG. 1. A schematic illustration of the cart-pendulum system to simulate humans' handling of a complex object such as a cup of hot coffee: (a) a conceptual model of a ball rolling inside a circular cup and (b) a nonlinear mechanical model of a pendulum attached to a moving cart.

based on dynamical systems, the cart-pendulum model, as shown in Fig. 1(b), has four variables: the displacement and velocity of the cart as well as the rotating angle and the angular velocity of the pendulum. This is thus a four-dimensional nonlinear dynamical system, subject to periodic driving. In a typical experimental setting, all four variables exhibit periodic or nearly periodic oscillations. It was found [2] that humans tend to select either a low-frequency or a high-frequency strategy to successfully handle the complex object. A remarkable finding was that, when a low-frequency (e.g., 0.66 Hz) strategy is used, the oscillations of the cart displacement and of the pendulum angle exhibit in-phase synchronization, but antiphase synchronization arises when a high-frequency (e.g., 1.18 Hz) strategy is selected.

In a common sense, when humans handle complex objects, the strategy used may not be fixed, depending on the individual and the environmental conditions. It can also occur that a human can switch the strategy in response to internal or external perturbations. In the particular virtual experimental setting [2], since both low- and high-frequency strategies are effective, it is conceivable that some participants in the virtual experiment did not hold on to a single strategy. How does a transition from in-phase synchronization associated with a low-frequency strategy to antiphase synchronization associated with a high-frequency strategy, or vice versa, occur? Especially, in the parameter space, is the boundary between the in-phase and antiphase synchronization regimes sharp, gradual, or sophisticated? In the virtual experimental study [2], the distribution of the low frequencies centers about 0.65 Hz while the center of the high-frequency distribution is about 1.2 Hz. The frequency value separating the two regimes is about 0.8 Hz. Does the transition between in-phase and antiphase synchronous dynamics coincide with this definition of the low- and high-frequency regimes?

Answers to these questions can provide insights into how soft robots may be designed to handle complex objects in an adaptive manner.

Synchronization is a universal phenomenon in nonlinear dynamical systems [9,10]. The following representative studies in different fields are particularly relevant to our work. In physics, antiphase behaviors and synchronization transitions occur in different types of systems. Earlier, antiphase states were observed in a multimode laser [11]. Synchronization of chaotic lasers was experimentally realized [12] and phase synchronization in a chaotic laser array was detected [13]. Synchronization transitions can also occur in arrays of Josephson junction systems [14]. In 2002, the then 336-year-old synchronization observations of Christiaan Huygens were reexamined in modern experiments and fully understood [15]. In physiology, synchronization and rhythmic processes are common [16]. In cardiology, phase locking in periodically stimulated cardiac cells is fundamental [17]. In chemistry, phase-lag synchronization in networks of coupled chemical oscillators was studied [18] and echo behavior in large populations of chemical oscillators was experimentally observed and theoretically understood [19].

In this paper, we develop an understanding of the transition between low- and high-frequency strategies based on the nonlinear dynamics of the cart-pendulum system. Following the experimental setting [2], we systematically investigate the dynamical states and bifurcations in the parameter plane of the forcing amplitude and frequency of the external periodic driving. Since the oscillations of the dynamical variables are not exactly sinusoidal, we use the Hilbert transform method to calculate the phase [20–24]. Our main finding is that, in the weakly forcing regime (e.g., the coffee cup is held loosely), the transition is abrupt in the sense that it can be enabled by a small change in the forcing frequency, but, beyond this forcing regime, an intermediate region in the frequency arises in which a complicated relation (neither in-phase nor antiphase synchrony) between the cart and pendulum motions arises. The abrupt transition in the regime of weak forcing can be analyzed by using a linearization of the system and explained using the theory of linear systems control, where the transition occurs precisely at the intrinsic frequency of the pendulum through a resonance. Beyond the weakly forcing regime, the system is nonlinear and the transition can be understood from bistability—a phenomenon that is ubiquitous in nonlinear dynamical systems [25–35]. In particular, in phase space, the in-phase and antiphase synchronous states can be viewed as two attractors, each with its own basin of attraction. In addition, there is a third attractor with a complicated relation between the phases of the cart and pendulum motions, which we name as the transition attractor. In the high-frequency regime, the antiphase attractor is dominant in that its basin of attraction contains most of the phase-space volume, whereas in the low-frequency

regime, the in-phase attractor dominates. Say we start from the high-frequency regime and gradually reduce the frequency. As the resonance frequency is approached, a transition attractor is born and the basin “volume” of the antiphase attractor begins to decrease while that of the former starts to increase. When the frequency starts to decrease from the resonance frequency, the in-phase attractor is born and its basin volume begins to increase while that of the transition attractor starts to decrease. Eventually, the entire phase space becomes the basin of the in-phase attractor for sufficiently low frequency. Remarkably, the boundaries separating the two basins of attraction, e.g., those of the transition and in-phase attractors, possess a fractal structure with transient chaos—the phenomenon of fractal basin boundaries [25,26,32]. Visually, the fractal structure is most dramatic near the resonance frequency. Overall, our results indicate that the transition between in-phase and antiphase synchronous attractors can occur upon a small amount of change in the frequency (in the weakly forcing regime, the required amount is near zero)—a mechanism that can be exploited for designing smart robots to adaptively handle complex objects in a changing environment.

II. FORCED CART-PENDULUM MODEL

The paradigmatic model [2] of humans’ handling of a complex object is a nonlinear dynamical system subject to external periodic forcing. In particular, a cup of hot coffee is described as a ball rolling inside a bowl, as shown in Fig. 1(a), which can be further simplified as the classical cart-pendulum system, with the motions of the bowl and the ball modeled by those of the cart and pendulum, respectively, as shown in Fig. 1(b). The motion of the cart is restricted to a straight line. The human handling of the coffee cup is described by an interaction “force” F_{inter} between the human and the cart (the coffee cup), which consists of a periodic driving term representing the human control and two terms that depend on the displacement and velocity of the cart, respectively. Quantitatively, the human control can be parameterized by the amplitude and frequency of the periodic forcing. The force acts on the cart, driving the cart to move with velocity \dot{x} , which in turn excites the pendulum, causing it to swing. The angular position θ of the pendulum is measured as the angle made with the $-y$ direction, which is positive counterclockwise, and the corresponding angular velocity is $\dot{\theta}$. For simplicity, the cart’s translation motion and the pendulum’s rotational motion are assumed [2] to be frictionless. The cart-pendulum system has two degrees of freedom: the horizontal displacement $x(t)$ of the cart and the oscillation angle $\theta(t)$ of the pendulum, giving rise to a four-dimensional phase space: $[x(t), \dot{x}(t), \theta(t), \dot{\theta}(t)]$. Because of the periodic driving, the whole system is five dimensional.

The system equations are

$$\dot{x} = \dot{x}, \quad (1)$$

$$\dot{\theta} = \dot{\theta}, \quad (2)$$

$$\ddot{x} = \frac{m_p d \dot{\theta}^2 \sin(\theta) + m_p g \sin(\theta) \cos(\theta) + F_{\text{inter}}}{m_c + m_p \sin^2(\theta)}, \quad (3)$$

$$\ddot{\theta} = -\frac{\ddot{x}}{d} \cos(\theta) - \frac{g}{d} \sin(\theta), \quad (4)$$

where $\mathbf{x} = [x_1, x_2, x_3, x_4]^T \equiv [x, \theta, \dot{x}, \dot{\theta}]^T \in \mathbb{R}^4$ denotes the state vector, m_c is the mass of the cart, m_p is the mass of the pendulum of length d , and g is Earth’s gravitational acceleration.

As described in Ref. [2], in the virtual experiment, the human tracks the desired cart position with a sinusoidal reference trajectory

$$x_{\text{des}}(t) = A \sin(2\pi f t + \pi/2),$$

which, for the cart-pendulum model, requires a sinusoidal driving force

$$F_{\text{input}}(t) = (m_c + m_p) \ddot{x}_{\text{des}}(t) = F \sin(2\pi f t + \pi/2),$$

where the forcing amplitude F is given by $F = -A(m_c + m_p)(2\pi f)^2$. Generally, due to the dynamic constraints of the hands and limbs of the human, there is a mismatch between the motion of the cart-pendulum system and human tracking: the human is unable to follow the reference command $F_{\text{input}}(t)$ exactly. This feature can be taken into account by passing the reference command F_{input} through a human-limb actuator model: a mass-spring system of stiffness K and damping coefficient B . The actuator model produces the interaction force F_{inter} that represents the force acting directly on the cart, which is given by [2]

$$F_{\text{inter}} = F_{\text{input}} - K(x - x_{\text{des}}) - B(\dot{x} - \dot{x}_{\text{des}}). \quad (5)$$

Values of all physical parameters of the model [2] are listed in Table I.

The model represented by Eqs. (1)–(4), adopted from the virtual experimental study of balancing a rolling ball

TABLE I. Values of physical parameters in the forced cart-pendulum model.

Parameter	Value
m_c	2.4 kg
m_p	0.6 kg
d	0.45 m
g	9.81 m/s ²
K	100 N/m
B	10 Ns/m

in a bowl [2,3], is idealized and has deficiencies. A major deviation from real coffee-cup carrying is that the participants of the virtual experiment can look at the coffee cup all the time. However, in the real world (as known by service providers at restaurants), the best way to carry a coffee cup or bowl of soup without spilling its contents is not to look at the liquid level. The virtual experiment [2,3] and the model thus do not capture this real feature.

From the point of view of control, the problem associated with carrying a coffee cup while looking at the liquid level is an example of “over control” [6]. That is, the nervous system is trying to correct small fluctuations in the fluid level that do not need to be corrected, a control strategy that makes the task more difficult to control. For balance control such as balancing a pole at the fingertip [4,8], too quick a response by a controller to a given deviation can lead to over control.

In general, in real coffee-cup carrying, time delays and noise are inevitably present in the human nervous system. A seminal mathematical study of the interplay among time delays, noise, and control was carried out by Milton *et al.* [6]. A finding was that such systems are controllable using readily implemented control strategies. For example, in the case of balance control, the human nervous system may have adopted a simple but robust control strategy: the system is simply allowed to drift until the controlled variable exceeds a threshold that initiates a corrective action. This result provides insights into humans’ remarkable ability in balance control. It was also suggested that over control can lead to destabilization when there is time delay. The cart-pendulum model Eqs. (1)–(4) for coffee-cup carrying derived from the virtual experiment [2,3] represents only a simplified description of the experiment because it does not include any time delay, and therefore is not suited for accounting for the over-control phenomenon that is likely to be present in the virtual experimental study and in the real world as well (e.g., coffee-cup carrying strategy utilized by a novice).

III. NUMERICAL RESULTS

A. In-phase and antiphase synchronization between the pendulum and cart

Figures 2(a)–2(c) display the representative time series of both the pendulum and the cart when the system is forced with the reference command amplitude $F = 5$ N for three different values of the driving frequency: $f = 0.6$ Hz, 0.7 Hz, and 0.8 Hz, respectively. For the relatively small frequency $f = 0.6$ Hz, the oscillations of the pendulum and cart are nearly perfectly sinusoidal and they are in phase, as shown in Fig. 2(a). In this case, there is phase synchronization between the pendulum and the cart. As the driving frequency is increased to $f = 0.7$ Hz, the oscillations of the pendulum remain sinusoidal, but for the cart, high-order harmonic oscillations have emerged, as shown

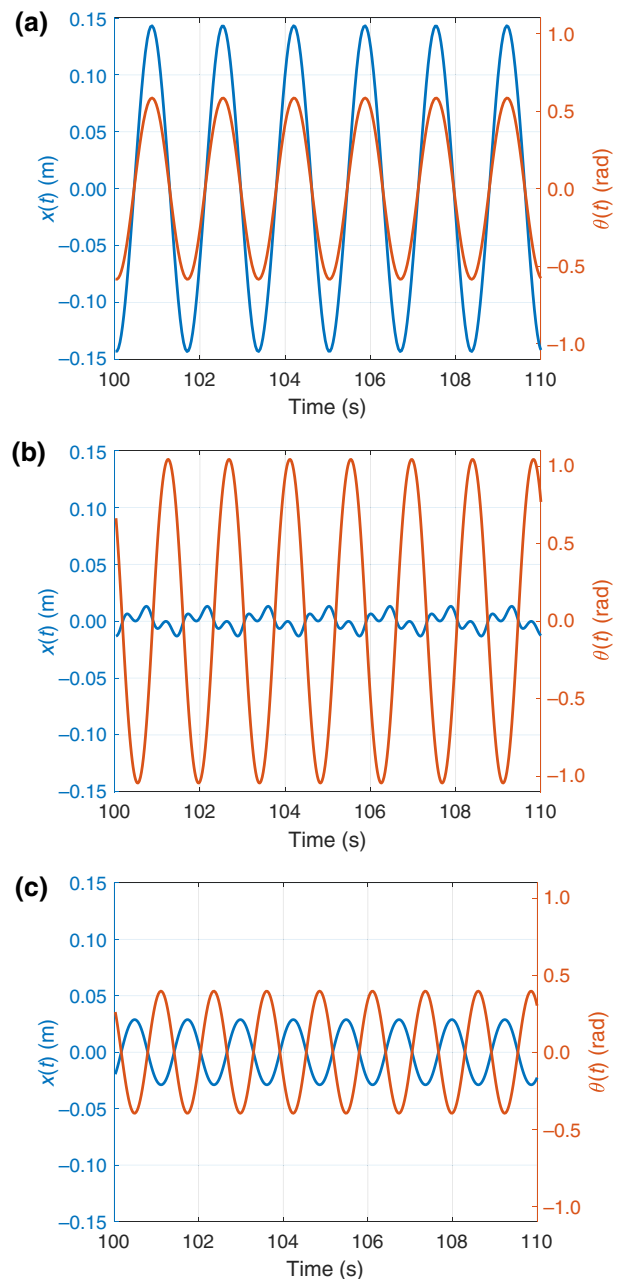


FIG. 2. Representative time series of cart position $x(t)$ (blue) and pendulum angular position $\theta(t)$ (orange) for forcing amplitude $F = 5$ N. (a)–(c) Driving frequencies $f = 0.6$ Hz, $f = 0.7$ Hz, and $f = 0.8$ Hz, respectively. There is in-phase synchronization between the pendulum and the cart for $f = 0.6$ Hz (a) and antiphase synchronization for $f = 0.8$ Hz (c).

in Fig. 2(b). In this case, for the cart, a unique and meaningful phase variable cannot be defined. As the driving frequency is further increased to $f = 0.8$ Hz, the oscillations of both the pendulum and cart are again sinusoidal, rendering existent well-defined phase variables for both. The surprising phenomenon is that there is now antiphase synchronization [36] between the pendulum and the cart,

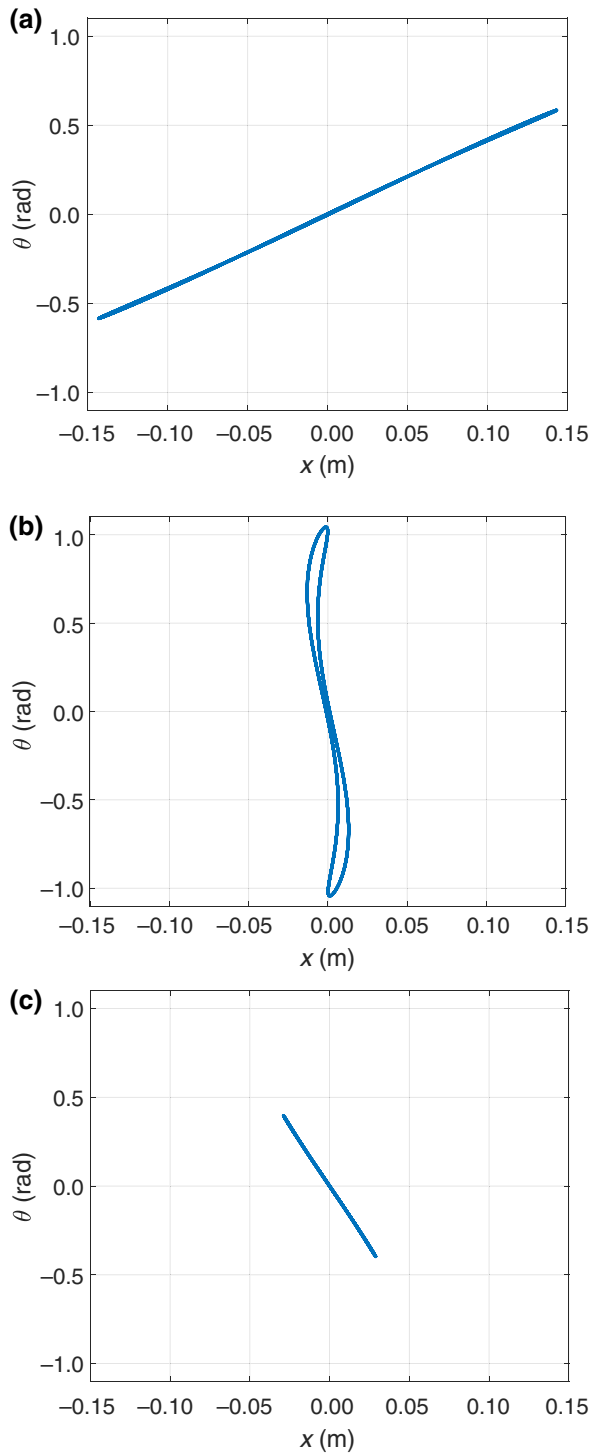


FIG. 3. Representative phase-plane trajectories of cart position $x(t)$ and pendulum angular position $\theta(t)$. (a)–(c) Driving frequencies $f = 0.6$ Hz, $f = 0.7$ Hz, and $f = 0.8$ Hz, respectively.

as shown in Fig. 2(c). The synchronous, asynchronous, and antisynchronous behaviors can also be visualized directly from the corresponding trajectories in the plane of the dynamical variables (x, θ) , as shown in Figs. 3(a)–3(c), respectively. For the lower frequency $f = 0.6$ Hz, the

trajectory falls on a straight line of a positive slope, indicating perfect phase synchronization, as shown in Fig. 3(a). In the opposite case of antiphase synchronization at $f = 0.8$ Hz, the trajectory again falls on a straight line but with a negative slope. For $f = 0.7$ Hz, the trajectory (x, θ) is not a line but a closed curve, indicating the lack of a unique phase correspondence. The behaviors demonstrated in Figs. 2 and 3 suggest that, as the driving frequency is decreased from $f = 0.8$ Hz to $f = 0.6$ Hz, a transition from antiphase to in-phase synchronization between the pendulum and cart has occurred.

For a frequency value within the transition regime, as exemplified by Figs. 2(b) and 3(b), the pendulum exhibits persistently sinusoidal oscillations with a large amplitude while the cart undergoes nonsinusoidal, small amplitude oscillations. For weak forcing, this behavior of the pendulum can be heuristically understood by analyzing the underlying linearized dynamical system through the mechanism of linear resonance near the natural frequency of the pendulum $\omega_n = \sqrt{g/d}$. Likewise, the small amplitude of cart oscillation can be explained as the result of a dynamic zero at the same resonance frequency (Sec. IV A).

To characterize the phase behaviors of the pendulum and cart more precisely, we use the standard Hilbert transform method. Letting $\phi_\theta(t)$ and $\phi_x(t)$ be the instantaneous phase variables underlying the oscillations of the pendulum and cart motions, respectively, we calculate the phase difference $\Delta\phi(t) \equiv |\phi_x(t) - \phi_\theta(t)|$. Figure 4(a) shows that, in the frequency regime of in-phase synchronization ($f = 0.6$ Hz), the phase difference is zero. For $f = 0.8$ Hz in the antiphase synchronization regime, we have $\Delta\phi(t) = \pi$, as shown in Fig. 4(c). In the regime of transition between in-phase and antiphase synchronization, a straightforward application of the Hilbert transform method leads to an oscillating phase difference, as shown in Fig. 4(b). This is due to the fact that, in this transition regime, the phase of the cart cannot be meaningfully defined. In fact, in this regime, the oscillations in the cart position contain a secondary rotational component in the plane of the analytic signal [22].

B. Transition between in-phase and antiphase synchronization—a global picture

To systematically study the transition between in-phase and antiphase synchronization behavior, we focus on the parameter plane of forcing frequency and amplitude (f, F) . In particular, we vary the frequency and amplitude in the ranges $(0.55, 0.8)$ Hz and $(0, 8)$ N, respectively, and place a uniform grid in the region. For each parameter pair, we calculate the phase difference $\Delta\phi$. If its value falls within $\pm\pi/10$ rad of zero or π , the parameter pair is regarded to be in the in-phase or antiphase synchronization regime, respectively; otherwise, the phase difference is inclusive and the parameter pair is deemed to

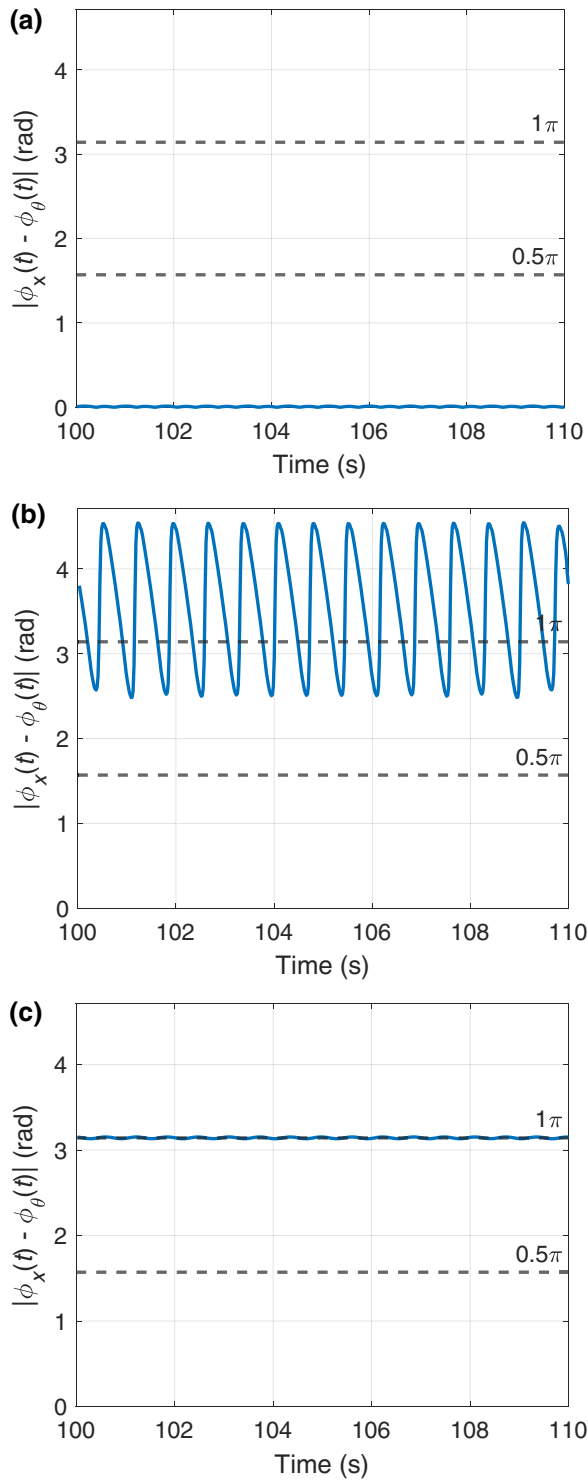


FIG. 4. Absolute difference in the instantaneous phase between the pendulum and the cart displacement. The forcing amplitude is $F = 5$ N. (a)–(c) Driving frequencies $f = 0.6$ Hz, $f = 0.7$ Hz, and $f = 0.8$ Hz, respectively.

belong to the transition region. Figure 5 displays the three distinct regions in the parameter plane: in-phase synchronization (blue), antiphase synchronization (turquoise), and

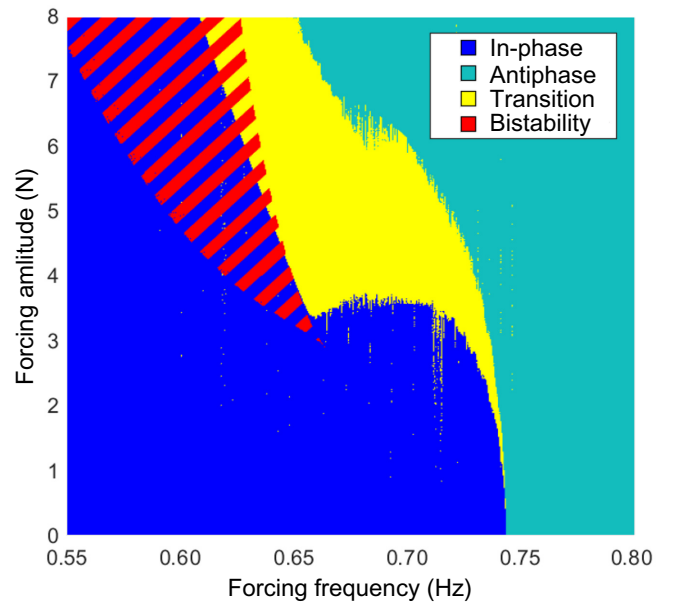


FIG. 5. Transition scenarios between in-phase and antiphase synchronization in the parameter plane of forcing frequency and amplitude. Blue represents the in-phase synchronization region in which the phase difference between the pendulum and cart is zero; turquoise represents the antiphase synchronization region in which the phase difference is π ; yellow represents the region in which the phase difference does not settle into a steady-state value. The initial condition is $x(0) = 0$, $\theta(0) = 0$, $\dot{x}(0) = 0$, and $\dot{\theta}(0) = 0$. There are two distinct transition scenarios: abrupt transition in the weakly forcing regime where the critical frequency value is the natural frequency of the pendulum, and gradual transition in which an intermediate frequency region of indeterminate phase difference arises between the in-phase and antiphase synchronization regions. The red stripes specify the region of bistability (to be discussed in Sec. IV B), calculated using initial conditions $x(0)$, $\theta(0)$, $\dot{x}(0)$, and $\dot{\theta}(0)$ —all chosen uniformly from the interval $[-2, 2]$.

transition region (yellow). For small forcing amplitudes, the yellow region diminishes, indicating that the transition between in-phase and antiphase synchronization through varying the forcing frequency is abrupt, where the transition point is nothing but the natural frequency of the pendulum $f_n = \omega_n/2\pi = 0.7431$ Hz. This behavior can be understood via a detailed analysis of the linearized dynamics (in Sec. IV A). Beyond the weakly forcing regime, the transition is not abrupt: there is a range of intermediate frequency values in which the phase difference does not settle into any steady-state value.

IV. ANALYSIS OF SYNCHRONOUS TRANSITION SCENARIOS

Figure 5 reveals two distinct transition scenarios that occur in the regimes of small and relatively large forcing amplitudes, respectively. In the weak forcing regime,

as the driving frequency varies, there is an abrupt transition between in-phase and antiphase synchronization. In this case, the cart-pendulum system can be approximated by a linear model and the abrupt transition can be understood based on the principle of linear resonance (Sec. IV A). Beyond the weak forcing regime, a transition region emerges between in-phase and antiphase synchronization. In this case, the system is nonlinear and the transition scenario can be explained through the phenomenon of bistability (Sec. IV B).

A. Abrupt transition between in-phase and antiphase synchronization in the weakly forcing regime

Under weak forcing, as the driving frequency is reduced, the transition from antiphase to in-phase synchronization is abrupt without an intermediate region with a different kind of attractor. We use linear control theory [37] to understand

this behavior. In the weak forcing regime, the linearized state space can be designated as

$$\mathbf{x} = [x, \theta, \dot{x}, \dot{\theta}, x_{\text{des}}, \dot{x}_{\text{des}}]^T, \quad (6)$$

$$\mathbf{u} = F_{\text{input}}, \quad (7)$$

$$\mathbf{y} = [x, \theta]^T, \quad (8)$$

where the two auxiliary states, x_{des} and \dot{x}_{des} from Eq. (5), are used, and \mathbf{u} can be regarded as a control signal. The linearized dynamical system subject to control can then be written as

$$\dot{\mathbf{x}} = \mathcal{A} \cdot \mathbf{x} + \mathcal{B} \cdot \mathbf{u}, \quad (9)$$

$$\mathbf{y} = \mathcal{C} \cdot \mathbf{x} + \mathcal{D} \cdot \mathbf{u}, \quad (10)$$

with the matrices given by

$$\mathcal{A} = \begin{bmatrix} 0 & 0 & 1 & 0 & 0 & 0 \\ 0 & 0 & 0 & 1 & 0 & 0 \\ -K/m_c & m_p g/m_c & -B/m_c & 0 & K/m_c & B/m_c \\ K/m_c d & -(g/d)(1 + m_p/m_c) & B/m_c d & 0 & -K/m_c d & -B/m_c d \\ 0 & 0 & 0 & 0 & 0 & 1 \\ 0 & 0 & 0 & 0 & 0 & 0 \end{bmatrix},$$

$$\mathcal{B} = \begin{bmatrix} 0 \\ 0 \\ 1/m_c \\ -1/m_c d \\ 0 \\ 1/(m_c + m_p) \end{bmatrix},$$

$$\mathcal{C} = \begin{bmatrix} 1 & 0 & 0 & 0 & 0 & 0 \\ 0 & 1 & 0 & 0 & 0 & 0 \end{bmatrix},$$

$$\mathcal{D} = \begin{bmatrix} 0 \\ 0 \end{bmatrix}.$$

A block diagram representation of the linear control system is shown in Fig. 6, where, for the summing junctions, the input is assumed to be additive unless indicated by a minus sign.

The beige subsystem P_θ from input torque τ_θ to the pendulum angle θ is the standard linearized hanging pendulum system with zero rotational damping, which has imaginary-axis poles at $\pm j\sqrt{g/d}$. The locations of these poles in the

innermost feedback path is a fundamental determinant of the relative dynamics between x and θ . Let T_{ab} denote the closed-loop transfer function map from signal a to signal b . The closed-loop maps from the force reference command F_{input} to cart position x and pendulum angle θ can then be written as $T_{F_{\text{input}}x}$ and $T_{F_{\text{input}}\theta}$, respectively. The transfer functions associated with the closed-loop maps are

$$T_{F_{\text{input}}x}(s) = \frac{1}{m_c} \frac{(s^2 + \frac{g}{d}) \left(s^2 + \frac{B}{m_c + m_p} s + \frac{K}{m_c + m_p} \right)}{s^2 \left(s^4 + \frac{B}{m_c} s^3 + \frac{(m_c + m_p)g + Kd}{m_c d} s^2 + \frac{Bg}{m_c d} s + \frac{Kg}{m_c d} \right)}, \quad (11)$$

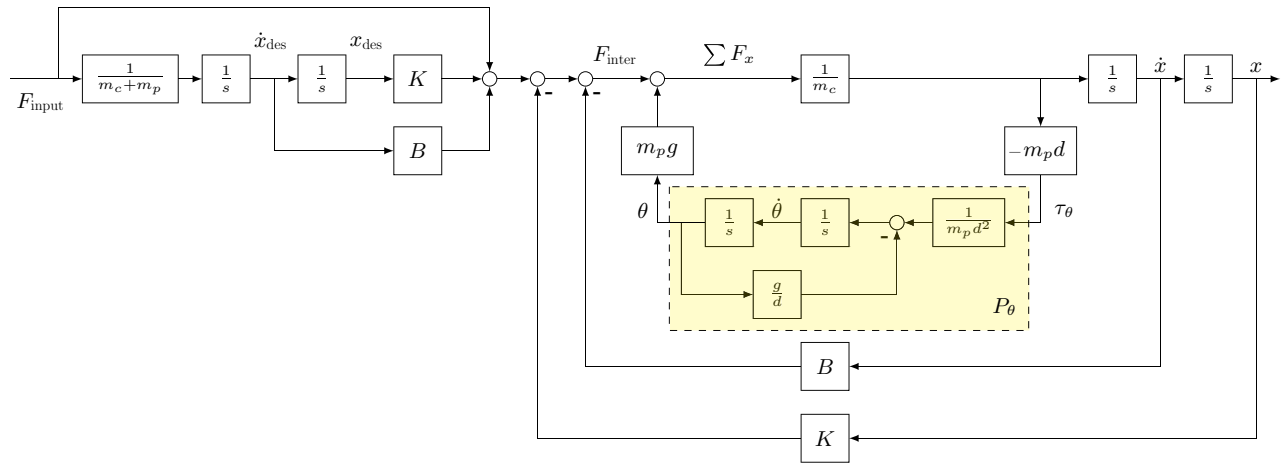


FIG. 6. Block diagram of the equivalent linear control system in the weak forcing regime. For summing junctions, the input is assumed to be additive unless otherwise indicated by a minus sign.

$$T_{F_{\text{input}}\theta}(s) = -\frac{1}{m_c d} \frac{\left(s^2 + \frac{B}{m_c + m_p} s + \frac{K}{m_c + m_p}\right)}{\left(s^4 + \frac{B}{m_c} s^3 + \frac{(m_c + m_p)g + Kd}{m_c d} s^2 + \frac{Bg}{m_c d} s + \frac{Kg}{m_c d}\right)}, \quad (12)$$

where $s = \sigma_0 + j\omega_0$ is the complex Laplace transform variable. The map $T_{F_{\text{input}}x}$ has imaginary-axis zeros at $\pm j\sqrt{g/d}$, due to the presence of the imaginary-axis resonant poles associated with P_θ embedded in the feedback path of the innermost loop in Fig. 6, i.e., the feedback loop associated with the second derivative of x . The map $T_{F_{\text{input}}x}$ also contains a double integrator, which is derived from the Newtonian dynamics of the cart in the absence of damping. The remaining poles and zeros arise from the feedback loops formed by the hand-coupling dynamics, which are associated with the actuator stiffness K and damping B . The map $T_{F_{\text{input}}\theta}$ does not feature the same imaginary-axis zeros at $\pm j\sqrt{g/d}$ because these zeros are canceled by the resonant poles in P_θ . It also lacks the double integrator of $T_{F_{\text{input}}x}$ associated with the Newtonian dynamics in x , which is expected. Otherwise, $T_{F_{\text{input}}\theta}$ has the same actuator poles and zeros as $T_{F_{\text{input}}x}$.

From the block diagram in Fig. 6, we can get the map $T_{x\theta}$ from x to θ as

$$T_{F_{\text{input}}\theta} = T_{x\theta} T_{F_{\text{input}}x},$$

where $T_{x\theta}$ can be obtained from Eqs. (11) and (12) as

$$T_{x\theta}(s) = -\frac{1}{d} \left(\frac{s^2}{s^2 + g/d} \right), \quad (13)$$

where $T_{x\theta}$ is independent of the actuator dynamics associated with the terms K and B . This can be seen from

manipulating Fig. 6 with minor block-diagram algebra. In particular, inserting a differentiator after x and reconnecting the B feedback path to the differentiated x reveals an inner network $T_{F_{\text{inter}}x}$. From the interaction force F_{inter} to x , we see that it is the standard linearized cart-pendulum system without actuator dynamics. The closed-loop map $T_{F_{\text{inter}}x}$ is unaffected by the external feedback, and so are any closed-loop maps of signals internal to $T_{F_{\text{inter}}x}$, i.e., $T_{x\theta}$. As a result, for low forcing amplitudes when the state \mathbf{x} stays near the origin and the linearized dynamics approximation is valid, the relative dynamics between the cart position x and pendulum angle θ see the same resonance structure, regardless of the hand-coupling dynamics that in general may vary from person to person.

Figure 7 shows the frequency response of the closed-loop map $T_{x\theta}$. It can be seen that, as the frequency increases, x and θ are perfectly in-phase until the resonant frequency $\sqrt{g/d}$, above which x and θ are exactly 180° out of phase. The attainment of the 180° phase shift is immediate, rendering the transition abrupt. This result agrees with that from the simulation of the full nonlinear system, as shown in Fig. 5, where the transition regime becomes increasingly narrow as the forcing amplitude decreases, which collapses to the resonant frequency of the pendulum when the forcing amplitude becomes sufficiently small. The linear control analysis thus provides an explanation for the abrupt transition between the low-frequency (in-phase) and high-frequency (antiphase) synchronous dynamics in the weakly forcing regime.

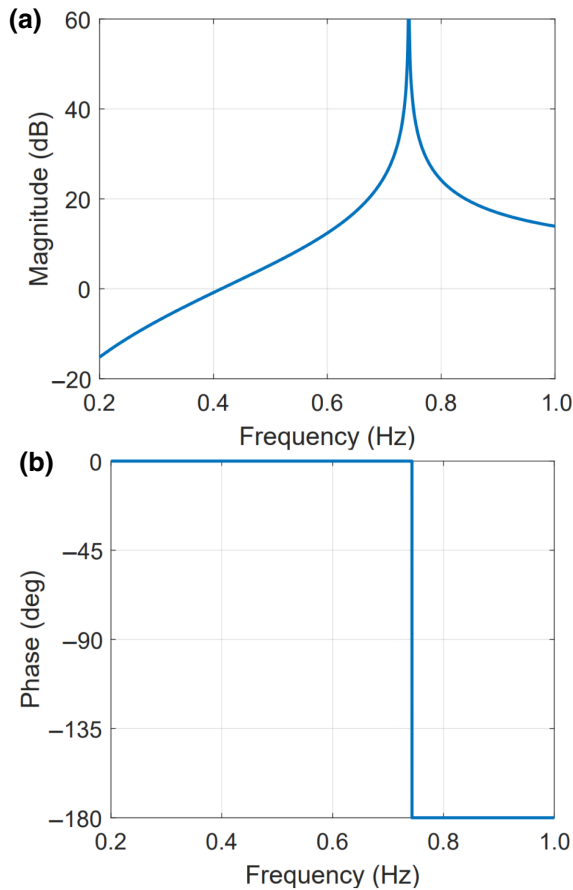


FIG. 7. Frequency response of $T_{x\theta}$. Right: magnitude response. Left: phase response.

Qualitatively, the dynamics of the linearized system subject to external forcing (control) can be described as follows. First, note that the map $T_{x\theta}$ has two zeros at dc (i.e., 0 Hz). This is because, for a constant input force F_{input} , the system dissipates any transient associated with the pendulum dynamics and behaves as a particle-mass system under a constant applied force. From Eq. (11), we see that the output at x takes the form of a parabola. However, from Eq. (12), the pendulum will settle into a constant position. As a result, $T_{x\theta}$ approaches zero at low frequencies as the x dynamics becomes dominant. Second, at the resonant frequency, the pendulum dynamics dominates. The imaginary-axis zeros in $T_{F_{\text{input}}x}$ from P_θ cause an infinite resonance peak in $T_{x\theta}$. Finally, at high frequencies, $T_{x\theta} \approx -1/d$ approaches a constant value. The constant high-frequency gain is an expected result since the pendulum subsystem h_θ and cart subsystem are both second order in nature. As a result, at high frequencies, the dynamical responses of both x and θ decay at the same rate and their relative gain approaches a constant value. This result can be seen concretely from Eqs. (11) and (12).

B. Synchronous transition scenario in the strong forcing regime

In the strong forcing regime, the transition between in-phase and antiphase synchronization is not abrupt: there is an intermediate frequency region in between the two types of synchronous dynamics. Numerically, we uncover the emergence of bistability about the intermediate frequency region, which provides a mechanism for the transition.

Multistability characterized by the coexistence of a number of attractors in the phase space is common in nonlinear dynamical systems [25–35,38]. In low-dimensional systems, there can be only a few coexisting attractors [25–29] or many [30,31]. Multistability can also arise in high-dimensional systems such as those described by nonlinear partial differential equations, e.g., an electrically driven silicon nanowire [33,39], and even in hybrid quantum-classical systems such as the coupled system of a ferromagnet and a topological insulator [35,40]. Controlling multistability has also been studied [30,34,41–43]. Multistability can also arise in solid-state physical systems such as semiconductor superlattices [38,44–46].

In the cart-pendulum system, for relatively large forcing amplitudes, e.g., $F > 3.3$ N, the system is highly nonlinear and bistability characterized by two coexisting attractors in the phase space arises. The parameter region in which bistability arises is indicated by the red stripes in Fig. 5. Part of this bistability region also overlaps with the transition region. Figure 8 shows the time-series and phase-space plots of the two distinct coexisting attractors.

To describe the observed bistability, we start from the parameter regions in which bistability is absent, i.e., almost all initial conditions lead to trajectories approaching a single attractor. There are two such “simple” regions: one on the left side of Fig. 5 and another on the right side. In the left “simple” region, the single attractor is associated with in-phase synchronization, as exemplified in Figs. 2(a) and 3(a). In the “simple” region on the right side, there is an antiphase synchronization attractor, as exemplified in Figs. 2(c) and 3(c). In the phase-space plane (x, θ) , both attractors have a nearly linear structure, but the in-phase attractor has a positive slope while the antiphase attractor has a negative slope, indicating nearly perfect positive and negative correlation between the dynamical variables $x(t)$ and $\theta(t)$, respectively.

As the parameters vary from the “simple” regions in Fig. 5 toward the central region, the phase relation between $x(t)$ and $\theta(t)$ becomes sophisticated, leading to some attractors with neither zero nor π phase difference but with “Lissajous” structure in the (x, θ) plane, as shown in Fig. 3(b). In fact, as revealed by Fig. 2(b), in the transition region, $\theta(t)$ remains sinusoidal but the waveform of $x(t)$ develops secondary oscillations, making ambiguous a proper definition of its phase, even though both signals are periodic. These Lissajous attractors are deformed from the antiphase attractors as the forcing frequency decreases

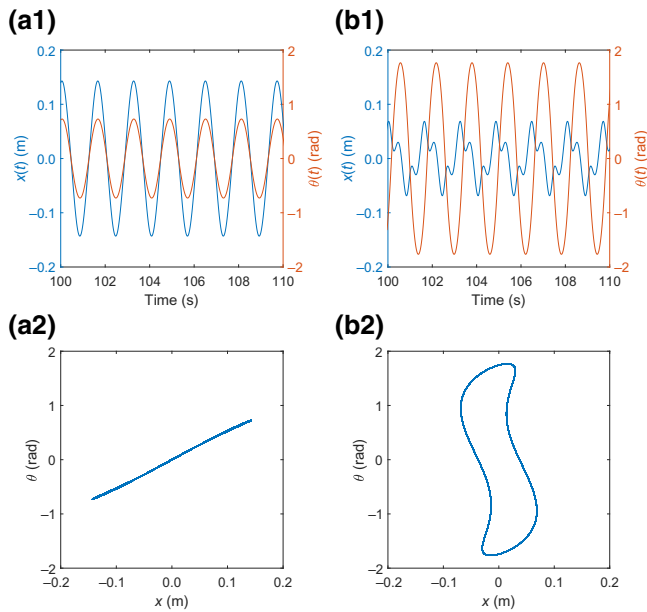


FIG. 8. Illustration of bistability. Shown are two distinct dynamical behaviors in the bistability region, which are observed for the same set of parameter values ($f = 0.62$ Hz and $F = 5$ N) but with different initial conditions. (a1),(a2) Waveforms $x(t)$ and $\theta(t)$ and the corresponding phase space plot, respectively, from the initial conditions $x(0) = 0$, $\theta(0) = 0$, $\dot{x}(0) = 0$, and $\dot{\theta}(0) = 0$. This is an in-phase attractor. It is not exactly sinusoidal, but is very close to. (b1),(b2) Waveforms $x(t)$ and $\theta(t)$ and the corresponding phase space plot, respectively, from the initial conditions $x(0) = 0.4$, $\theta(0) = 0.3$, $\dot{x}(0) = -1.1$, and $\dot{\theta}(0) = 1.7$. This is a “Lissajous” attractor. In the bistability regime, two distinct attractors as exemplified in (a2) and (b2) coexist.

toward the central region. The in-phase attractors also have deformation as the forcing frequency increases toward the central region. But their deformation is much weaker and does not make the attractor very different from sinusoidal.

About the same central region, we find a region with bistability, marked with red stripes in Fig. 5. In this region, the system may reach both the in-phase attractor and the Lissajous attractor depending on the initial states, as shown in Fig. 8. We further find that associated with bistability is fractal basin boundaries, as shown in Fig. 9.

The transition scenario can then be described as follows. For a fixed forcing amplitude, we start from the high-frequency region. As the frequency reduces, the antiphase attractor is continuously deformed until when the π phase difference can no longer be approximately maintained. This event marks the right numerical boundary between the yellow and turquoise regions in Fig. 5. Below but near this empirical boundary, there is only one attractor in the phase space, the Lissajous attractor. At the boundary between the yellow and red-striped regions, the in-phase attractor is born, which is a periodic attractor of period one in the phase space (or a fixed point in some Poincaré surface of section). In the frequency interval

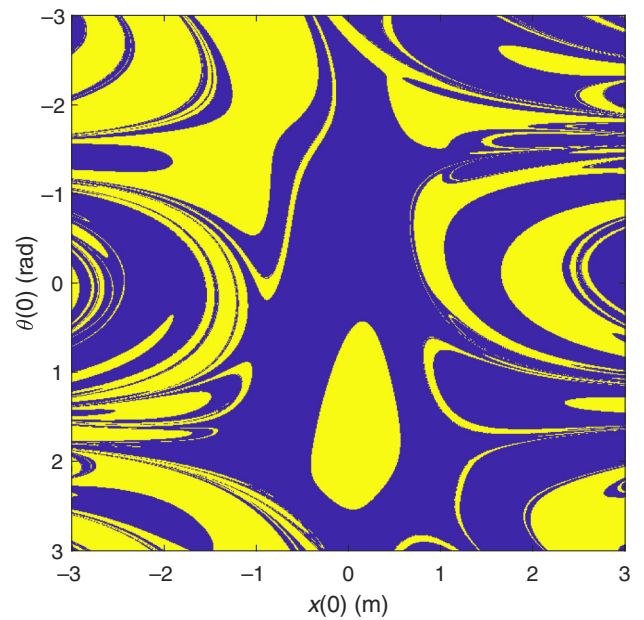


FIG. 9. Fractal basin boundaries. In the parameter region where there is bistability, the boundaries between the basins of attraction of the two coexisting attractors exhibit an apparently fractal structure. The parameter values are $f = 0.62$ Hz, $F = 7$ N, $\dot{x}(0) = 1$, and $\dot{\theta}(0) = 0.5$. The yellow regions are the basin of the in-phase attractor, and the blue regions represent the basin of the “Lissajous” attractor as exemplified in Fig. 8(b2).

defined by the red-striped region, there are two coexisting attractors, the deformed Lissajous attractor and the in-phase periodic attractor, signifying bistability. As the frequency is reduced from the right boundary of the bistability region, the basin of the in-phase attractor expands while that of the deformed attractor shrinks. At the left boundary of the bistability region, the basin of the Lissajous attractor diminishes, leaving the in-phase attractor as the only attractor in the system with its basin of attraction being the entire phase space. This nonlinear dynamical transition scenario is illustrated in Fig. 10, where a numerical bifurcation diagram is shown in terms of the local maxima of the angle $\theta(t)$ (a) and cart position $x(t)$ (b). Note that the boundary between the Lissajous and antiphase attractors is determined by the emergence of new local maxima of $x(t)$.

The results in Fig. 10 explain why the bistability region in Fig. 5 appears on the left side of the transition region. As the driving frequency is reduced, there are three critical values of interest: $f_1^c < f_2^c < f_3^c$, marked by the left, middle, and right left vertical dashed lines in Fig. 10(b), respectively. First, note that the Lissajous attractor is a continuation of the antiphase attractor, which arises at f_3^c . Second, the in-phase attractor is the result of a saddle-node bifurcation as the driving frequency is reduced, which occurs at $f_2^c < f_3^c$. The bistability region starts at f_2^c where a basin of the in-phase attractor is born. As f decreases

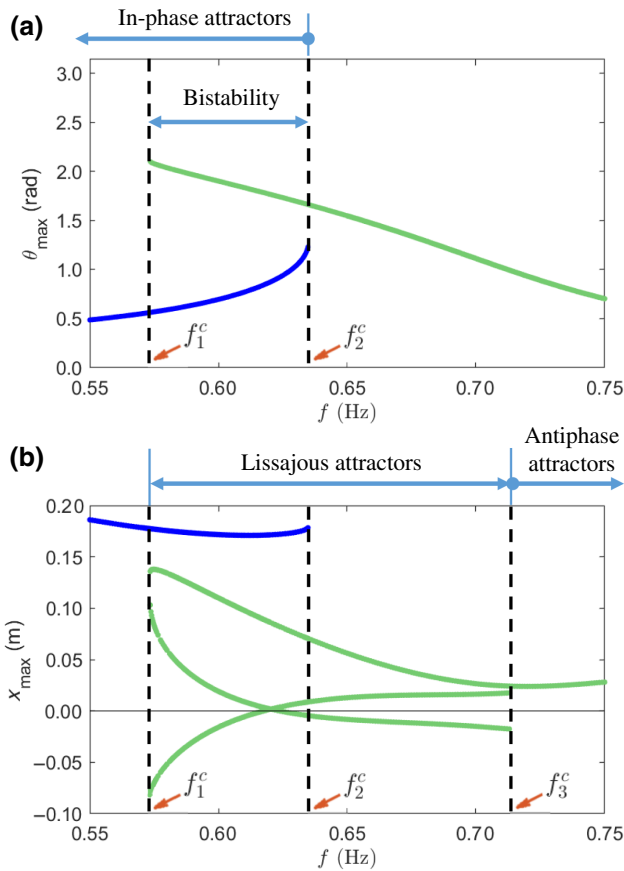


FIG. 10. Transition scenario from antiphase to in-phase attractors through bistability in the nonlinear regime. (a) Bifurcation diagram of the two attractors (in blue and green) for $F = 6$ N in terms of the maximum value of the pendulum angle. (b) Bifurcation diagram in terms of the maximum value of the cart displacement. There are four distinct parameter regions, which are distinguished by the three vertical black dashed lines. The boundary between the Lissajous and antiphase attractors is determined by the emergence of new local maxima of x . For a fixed value of a relatively large forcing amplitude, as the driving frequency is reduced, the system undergoes the following transition sequence: antiphase attractor \rightarrow Lissajous attractor \rightarrow bistability characterized by the coexistence of a Lissajous attractor and an in-phase attractor \rightarrow in-phase attractor.

from f_2^c , this basin expands but that of the Lissajous attractor shrinks. Bistability ends at f_1^c , at which the basin of the Lissajous attractor diminishes. These observations indicate that, because bistability is associated with the birth of the in-phase attractor, the corresponding parameter interval is contained in the interval of the in-phase attractor. As a result, the bistability region emerges toward the left side of Fig. 5.

V. DISCUSSION

Humans have the ability to handle complex objects such as a cup of hot coffee while walking. Such an object is complex because the coffee, a thermally excited fluid in

a confinement, has its own motion. The fluid motion interacts with the cup that is held by a human hand. As humans, we take this ability as natural and for granted, and few of us have actually realized that this system is nonlinear and the underlying dynamics can be quite complicated. Curiosity demands an understanding of the dynamical mechanism of this “coffee-cup” problem. More importantly, such an understanding is fundamental to designing soft robots capable of handling complex objects.

Recent virtual experiments have revealed [2,3] two distinct stable modes in humans’ handling of a complex object: in-phase and antiphase synchronization in the low- and high-frequency regimes, respectively. In particular, in the low-frequency regime as exemplified by a slowly walking human holding a cup of coffee, the motion of the hot fluid and the movement of the human hand are perfectly in phase. However, our experience stipulates that it is still possible to hold a cup of coffee when we walk fast. It turns out that the mode of operation in this relatively high-frequency regime is antiphase synchronization [2,3] where the fluid and human hand motions are exactly 180° out of phase. It is possible that humans are able to use both strategies skillfully and to switch from one strategy to another smoothly (perhaps without even realizing it). To uncover how this transition occurs from a dynamical point of view is the main contribution of this paper.

Utilizing a nonlinear cart-pendulum system as a justified computational model [2,3] to simulate the humans’ handling of a complex object, where the human and coffee motions correspond to those of the cart and pendulum, respectively, we unveil the transition scenarios between the in-phase and antiphase behaviors. In particular, in the regime of weak forcing (e.g., when the coffee cup is not held so tightly), the transition can be quite abrupt in the sense that a small change in the frequency can immediately result in a switch between the two strategies. However, when forcing is relatively strong (e.g., when the coffee cup is tightly held), a sizable change in the driving frequency is required for the transition. In fact, in this case, a region of transition arises in which the phase relation between the cart and pendulum is quite sophisticated. We have demonstrated that the abrupt transition in the weakly forcing regime can be understood by exploiting linear control theory and the transition scenario in the strongly forcing regime is the result of nonlinear dynamics through the emergence of bistability with fractal basin boundaries.

We note that the bistability phenomenon uncovered here was not recognized in the pioneering papers on coffee-cup carrying as a prototypical model for human complex object control [1–3]. A possible virtual experimental test of this phenomenon is to set the forcing amplitude and frequency in the bistability parameter region (the red-striped region in Fig. 5), to use a large number of initial conditions to start multiple experimental trials, and to record the relative movement of the human hand and the virtual ball. If, for

a given trial, this relative movement gives the phase relation as in Figs. 8(a1) and 8(a2), the system has settled into the in-phase attractor. However, if the relative movement leads to a more complicated phase relationship as exemplified by Figs. 8(b1) and 8(b2), the system has landed on the coexisting, phase-unsynchronized attractor for the trial. A large number of trials giving complementary fractions of settling into the two distinct attractors would be unequivocal evidence of bistability.

The transition scenarios uncovered together with a physical understanding of the underlying dynamical mechanisms of how humans handle complex objects can be exploited to inform the development of better soft robots. It is conceivable that, in the not-too-distant future, robots would be deployed in various applications of complex object handling or control that require coordination and movement control that humans do quite well. For the classic example of handling a cup of hot coffee while walking, our findings suggest the following principle when designing a soft robot. If the robot is designed to walk at a relatively small stride length, which roughly corresponds to a small forcing amplitude in the cart-pendulum model, then the underlying dynamics will be approximately linear and the frequency of walking can be arbitrary to generate either an in-phase or an antiphase behavior to ensure smooth handling of the coffee cup because, in this case, a transition region is absent between the two types of synchronous motions. However, if a relatively large stride length is desired (corresponding to a large forcing amplitude) then the frequency interval associated with the transition region should be avoided, because the complicated phase relation between the robot and the complex object there can ruin the smooth handling of the latter.

In addition to the model deficiencies in relation to the absence of time delay and the over-control problem discussed at the end of Sec. II, there is another possible difficulty with model (1)–(4). In particular, our dynamical analysis of the model suggests that humans are able to switch abruptly and efficiently from one synchronous attractor to another. However, at the present there is no experimental data of human movement characteristics collected in a way that can be compared with this prediction. It is possible that humans are not capable of making such movements. A problem with quick movements is how to minimize the jerk (third derivative), which was discussed in the context of pole balancing at the fingertip [4,8]. Experiences tell us that, for balancing a stick at the fingertip, the human finger movements can be quite quick, but this may not be the case for coffee-cup carrying. We hope that our finding will motivate experimental studies in this direction.

VI. ACKNOWLEDGMENTS

This work is supported by the ONR under Grant No. N00014-21-1-2323.

- [1] H. C. Mayer and R. Krechetnikov, Walking with coffee: Why does it spill?, *Phys. Rev. E* **85**, 046117 (2012).
- [2] P. Maurice, N. Hogan, and D. Sternad, Predictability, force, and (anti)resonance in complex object control, *J. Neurophysiol.* **120**, 765 (2018).
- [3] S. Bazzi, J. Ebert, N. Hogan, and D. Sternad, Stability and predictability in human control of complex objects, *Chaos* **28**, 103103 (2018).
- [4] J. L. Cabrera and J. G. Milton, On-Off Intermittency in a Human Balancing Task, *Phys. Rev. Lett.* **89**, 158702 (2002).
- [5] J. L. Cabrera and J. G. Milton, Human stick balancing: Tuning Lévy flights to improve balance control, *Chaos* **14**, 691 (2004).
- [6] J. G. Milton, J. L. Cabrera, and T. Ohira, Unstable dynamical systems: Delays, noise and control, *Europhys. Lett.* **83**, 48001 (2008).
- [7] J. G. Milton, J. L. Cabrera, T. Ohira, S. Tajima, Y. Tonosaki, C. W. Eurich, and S. A. Campbell, The time-delayed inverted pendulum: Implications for human balance control, *Chaos* **19**, 026110 (2009).
- [8] J. G. Milton, R. Meyer, M. Zhvanetsky, S. Ridge, and T. Insperger, Control at stability's edge minimizes energetic costs: Expert stick balancing, *J. R. Soc. Interface* **13**, 20160212 (2016).
- [9] L. M. Pecora and T. L. Carroll, Synchronization in Chaotic Systems, *Phys. Rev. Lett.* **64**, 821 (1990).
- [10] A. Pikovsky, M. Rosenblum, and J. Kurths, *Synchronization: A Universal Concept in Nonlinear Sciences* (Cambridge University Press, New York, 2001).
- [11] K. Wiesenfeld, C. Bracikowski, G. James, and R. Roy, Observation of Antiphase States in a Multimode Laser, *Phys. Rev. Lett.* **65**, 1749 (1990).
- [12] R. Roy and K. S. Thornburg, Experimental Synchronization of Chaotic Lasers, *Phys. Rev. Lett.* **72**, 2009 (1994).
- [13] D. J. DeShazer, R. Breban, E. Ott, and R. Roy, Detecting Phase Synchronization in a Chaotic Laser Array, *Phys. Rev. Lett.* **87**, 044101 (2001).
- [14] K. Wiesenfeld, P. Colet, and S. H. Strogatz, Synchronization Transitions in a Disordered Josephson Series Array, *Phys. Rev. Lett.* **76**, 404 (1996).
- [15] M. Matthew Bennett, M. F. Schatz, H. Rockwood, and K. Wiesenfeld, Huygens's clocks, *Proc. R. Soc. Lond. A* **458**, 563 (2002).
- [16] L. Glass, Synchronization and rhythmic processes in physiology, *Nature* **410**, 277 (2001).
- [17] M. R. Guevara, L. Glass, and A. Shrier, Phase locking, period-doubling bifurcations, and irregular dynamics in periodically stimulated cardiac cells, *Science* **214**, 1350 (1981).
- [18] J. F. Totz, R. Snari, D. Yengi, M. R. Tinsley, H. Engel, and K. Showalter, Phase-lag synchronization in networks of coupled chemical oscillators, *Phys. Rev. E* **92**, 022819 (2015).
- [19] T. Chen, M. R. Tinsley, E. Ott, and K. Showalter, Echo Behavior in Large Populations of Chemical Oscillators, *Phys. Rev. X* **6**, 041054 (2016).
- [20] M. G. Rosenblum, A. S. Pikovsky, and J. Kurths, Phase Synchronization of Chaotic Oscillators, *Phys. Rev. Lett.* **76**, 1804 (1996).

- [21] N. E. Huang, Z. Shen, S. R. Long, M. C. Wu, H. H. Shih, Q. Zheng, N.-C. Yen, C. C. Tung, and H. H. Liu, The empirical mode decomposition and the Hilbert spectrum for nonlinear and non-stationary time series, *Proc. R. Soc. Lond. A* **454**, 903 (1998).
- [22] T. Yalçınkaya and Y.-C. Lai, Phase Characterization of Chaos, *Phys. Rev. Lett.* **79**, 3885 (1997).
- [23] Y.-C. Lai, Analytic signals and the transition to chaos in deterministic flows, *Phys. Rev. E* **58**, R6911 (1998).
- [24] L. Huang, X. Ni, W. L. Ditto, M. Spano, P. R. Carney, and Y.-C. Lai, Detecting and characterizing high frequency oscillations in epilepsy – a case study of big data analysis, *R. Soc. Open Sci.* **4**, 160741 (2017).
- [25] C. Grebogi, S. W. McDonald, E. Ott, and J. A. Yorke, Final state sensitivity: An obstruction to predictability, *Phys. Lett. A* **99**, 415 (1983).
- [26] S. W. McDonald, C. Grebogi, E. Ott, and J. A. Yorke, Fractal basin boundaries, *Physica D* **17**, 125 (1985).
- [27] Y.-C. Lai and C. Grebogi, Intermingled basins and two-state on-off intermittency, *Phys. Rev. E* **52**, R3313 (1995).
- [28] Y.-C. Lai, C. Grebogi, J. A. Yorke, and S. Venkataramani, Riddling Bifurcation in Chaotic Dynamical Systems, *Phys. Rev. Lett.* **77**, 55 (1996).
- [29] Y.-C. Lai and C. Grebogi, Noise-Induced Riddling in Chaotic Dynamical Systems, *Phys. Rev. Lett.* **77**, 5047 (1996).
- [30] U. Feudel and C. Grebogi, Multistability and the control of complexity, *Chaos* **7**, 597 (1997).
- [31] U. Feudel and C. Grebogi, Why are Chaotic Attractors Rare in Multistable Systems?, *Phys. Rev. Lett.* **91**, 134102 (2003).
- [32] Y.-C. Lai and T. Tél, *Transient Chaos – Complex Dynamics on Finite Time Scales* (Springer, New York, 2011).
- [33] X. Ni, L. Ying, Y.-C. Lai, Y. Do, and C. Grebogi, Complex dynamics in nanosystems, *Phys. Rev. E* **87**, 052911 (2013).
- [34] A. N. Pisarchik and U. Feudel, Control of multistability, *Phys. Rep.* **540**, 167 (2014).
- [35] G.-L. Wang, H.-Y. Xu, and Y.-C. Lai, Nonlinear dynamics induced anomalous Hall effect in topological insulators, *Sci. Rep.* **6**, 19803 (2016).
- [36] L.-Y. Cao and Y.-C. Lai, Antiphase synchronism in chaotic systems, *Phys. Rev. E* **58**, 382 (1998).
- [37] W. J. Rugh, *Linear Systems Theory* (Prentice-Hall Inc., Upper Saddle River, New Jersey, 1996).
- [38] L. Ying, D. Huang, and Y.-C. Lai, Multistability, chaos, and random signal generation in semiconductor superlattices, *Phys. Rev. E* **93**, 062204 (2016).
- [39] Q. Chen, L. Huang, Y.-C. Lai, C. Grebogi, and D. Dietz, Extensively chaotic motion in electrostatically driven nanowires and applications, *Nano Lett.* **10**, 406 (2010).
- [40] G.-L. Wang, H.-Y. Xu, and Y.-C. Lai, Emergence, evolution, and control of multistability in a hybrid topological quantum/classical system, *Chaos* **28**, 033601 (2018).
- [41] Z. Kovács, K. G. Szabó, and T. Tél, in *Nonlinearity and Chaos in Engineering Dynamics*, edited by J. M. T. Thompson and S. R. Bishop (John Wiley and Sons, Chichester, England, 1994), p. 155.
- [42] Y.-C. Lai, Driving trajectories to a desirable attractor by using small control, *Phys. Lett. A* **221**, 375 (1996).
- [43] A. N. Pisarchik, Controlling the multistability of nonlinear systems with coexisting attractors, *Phys. Rev. E* **64**, 046203 (2001).
- [44] F. Prengel, A. Wacker, and E. Schöll, Simple model for multistability and domain formation in semiconductor superlattices, *Phys. Rev. B* **50**, 1705 (1994).
- [45] N. G. Sun and G. P. Tsironis, Multistability of conductance in doped semiconductor superlattices, *Phys. Rev. B* **51**, 11221 (1995).
- [46] A. Amann, A. Wacker, L. L. Bonilla, and E. Schöll, Dynamic scenarios of multistable switching in semiconductor superlattices, *Phys. Rev. E* **63**, 066207 (2001).